arXiv:1005.1343v1 [cond-mat.soft] 8 May 2010

Brownian motion of a self-propelled particle

Borge ten Hagen,[1,*] Sven van Teeffelen,[2] and Hartmut Löwen[1,†]

[1] *Institut für Theoretische Physik II: Weiche Materie, Heinrich-Heine-Universität Düsseldorf, Universitätsstr. 1, 40225 Düsseldorf, Germany*

[2] *Department of Molecular Biology, Princeton University, Princeton, NJ 08544, USA*

(Dated: May 11, 2010)

Overdamped Brownian motion of a self-propelled particle is studied by solving the Langevin equation analytically. On top of translational and rotational diffusion, in the context of the presented model, the "active" particle is driven along its internal orientation axis. We calculate the first four moments of the probability distribution function for displacements as a function of time for a spherical particle with isotropic translational diffusion as well as for an anisotropic ellipsoidal particle. In both cases the translational and rotational motion is either unconfined or confined to one or two dimensions. A significant non-Gaussian behavior at finite times t is signalled by a non-vanishing kurtosis $\gamma(t)$. To delimit the super-diffusive regime, which occurs at intermediate times, two time scales are identified. For certain model situations a characteristic t^3 behavior of the mean square displacement is observed. Comparing the dynamics of real and artificial microswimmers like bacteria or catalytically driven Janus particles to our analytical expressions reveals whether their motion is Brownian or not.

PACS numbers: 82.70.Dd, 05.40.Jc

I. INTRODUCTION

There are numerous realizations of self-propelled particles [1, 2] in nature ranging from bacteria [3–10] and spermatozoa [11–13] to artificial colloidal microswimmers. The latter are either catalytically driven [14–19] or navigated by external magnetic fields [20–22], but also biomimetic propulsion mechanisms can be exploited [23]. On the macroscopic scale, vibrated polar granular rods [24–26] and even pedestrians [27] provide more examples of "active" particles [28, 29]. A suitable framework for theoretical modeling of self-propellers is provided by the traditional Langevin theory of an anisotropic particle with translational and orientational diffusion including an effective internal force [30, 31] in the overdamped Brownian dynamics [32, 33]. The direction of the theoretically assumed internal propulsion force (corresponding to an imposed mean propagation speed) fluctuates according to rotational Brownian motion [34–36]. It is a challenging question whether real self-propelled particles can at least in a rough way be covered according to this simple Brownian picture. While for "passive" ellipsoidal particles a comparison revealed very good agreement with the picture of Brownian dynamics [37–39], this has never been undertaken for self-propellers. Any deviations point to the relevance of hydrodynamic interactions, non-Gaussian noise, or fluctuating internal forces which are beyond simple Brownian motion.

Despite its simplicity, the Brownian motion of anisotropic particles [40–42] has only been considered in the absence of internal driving forces either in the bulk [37, 43] or in an external force field derivable from a potential [44]. For "passive" rodlike particles the Smoluchowski-Perrin equation [34, 45] has been solved exactly in two [46] as well as in three [47] dimensions. With regard to self-propellers, so far analytical results are only available if the orientation vector is confined to two dimensions. For rodlike particles [48, 49] the first two [32], and for spherical particles the first four [50] moments of the probability distribution function for displacements were calculated. In this paper, we close the remaining gaps by presenting a comprehensive model and calculating the first four moments of the displacement distribution function for all relevant situations. First, we provide analytical results for an anisotropic self-propelled Brownian particle in two dimensions. Furthermore, both the situations of an isotropic and of an anisotropic particle are extended to the full three-dimensional case where the orientation vector is unconfined.

Studying the mean square displacement reveals a super-diffusive regime at intermediate times, which is characterized by a t^2 time dependence for most cases and beyond that by a t^3 behavior for some special cases. Moreover, two time scales that delimit the super-diffusive regime are identified. These can be extracted from the results for the mean square displacement or from the normalized fourth cumulant (kurtosis) $\gamma(t)$ of the probability distribution function for displacements, which measures the non-Gaussian behavior as a function of time t. For small and very large times, the kurtosis vanishes indicating Gaussian behavior, but due to both particle anisotropy and self-propulsion, $\gamma(t)$ is non-vanishing for intermediate times. While Han and coworkers [37] found the kurtosis of "passive" particles to be positive for $t > 0$ with a simple maximum at finite time [37], here we find that a propulsive force tends to make the kurtosis negative. There is a rich structure in $\gamma(t)$ revealing different

* bhagen@thphy.uni-duesseldorf.de

† hlowen@thphy.uni-duesseldorf.de

non-Gaussian behavior at different time scales. Quite generally, the propelling force induces a negative massive long-time tail in $\gamma(t)$ which tends to zero as $1/t$. This prediction can in principle be verified in experiments on self-propelled particles.

The paper is organized as follows: In Sec. II we present and motivate the various model situations that are considered in Secs. III to VI of this paper. In each case the first four displacement moments are calculated analytically and the results are analysed based on appropriate figures. Finally, we conclude and give an outlook on further expansion of our model in Sec. VII.

II. REMARKS ABOUT THE VARIOUS MODEL SITUATIONS

In this section, we give an overview of the situations to which the model is applied in this paper (see also Fig. 1). In general, the model consists of an isotropic or anisotropic self-propelled particle which undergoes completely overdamped Brownian motion. To describe the propulsion mechanism on average, we theoretically assume an effective internal force $\mathbf{F} = F\hat{\mathbf{u}}$ that is included in the Langevin equation. The orientation vector $\hat{\mathbf{u}}$ is introduced to specify the direction of the self-propulsion. Depending on the number of translational degrees of freedom, in some of the cases to be covered this force is projected either onto a linear channel or onto a two-dimensional plane. To characterize the different situations depending on the number of degrees of freedom of the particle, we introduce the following notation: The (D, d, σ)-model refers to the situation with D translational degrees of freedom and d orientational degrees of freedom. The possible values for these parameters are $D \in \{1, 2, 3\}$ and $d \in \{1, 2\}$. The parameter $\sigma \in \{s, e\}$ refers to the shape of the particle. While $\sigma = s$ relates to a spherical particle, for an ellipsoidal particle $\sigma = e$ is used. When no specific value is given for one of these parameters, we refer to the group of models with an arbitrary value for that parameter.

We will first refer to the $(D, 1, s)$-model, which is depicted in Fig. 1(a) (theoretical investigation in Sec. III). This system consists of a self-propelled spherical particle whose rotational motion is constrained to a two-dimensional plane. To study the behavior of the particle, we first refer to the one-dimensional translation in x-direction (Secs. III A to III C). In experiment, this situation can be achieved by confining swimmers by means of external optical fields [51, 52], for example. After investigating this $(1, 1, s)$-model the results can easily be transferred to the two-dimensional case ($(2, 1, s)$-model), which is done in Sec. III D. This model situation is especially useful to describe the motion of a self-propelled particle on a substrate.

As the assumption of spherical particles is not justifiable in many experimental situations, the model is generalized to ellipsoidal particles (see Fig. 1(b)) in Sec. IV by investigating the $(D, 1, e)$-model. The more complicated coupling between rotational and translational motion as opposed to spherical particles leads to qualitatively different results.

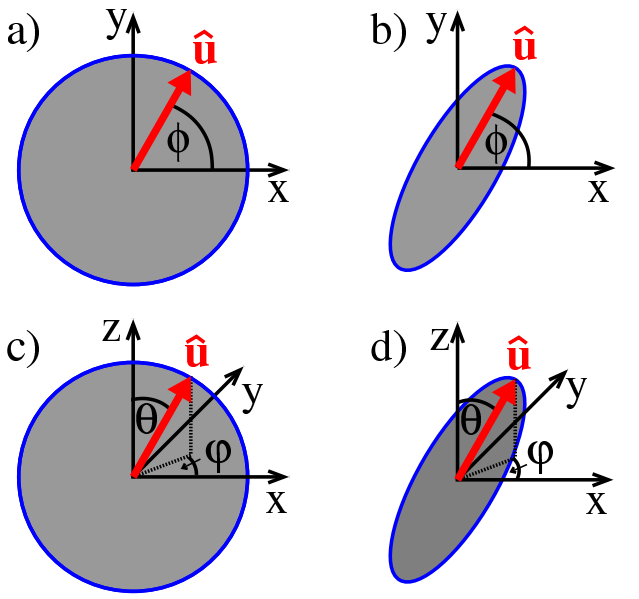

FIG. 1. (Color online) Sketch of the various situations to which the model is applied: a) $(D, 1, s)$-model, b) $(D, 1, e)$-model, c) $(D, 2, s)$-model and d) $(D, 2, e)$-model. The notation is explained in the text. For $D = 1$ in subfigures (a) and (b) and for $D < 3$ in subfigures (c) and (d), the effective driving force along the particle orientation $\hat{\mathbf{u}}$ is projected onto the respective number of translational dimensions. To cover the $(1, 1, s)$-model, for example, in subfigure (a) only the motion in the x-direction is considered.

Besides particles moving on a substrate with one orientational degree of freedom, we study freely rotating self-propelled particles. Here, the case of free translational motion in the bulk ($(3, 2, \sigma)$-model) is interesting as well as situations in which the translation of the particle is constrained either to a linear channel ($(1, 2, \sigma)$-model) or to a two-dimensional plane ($(2, 2, \sigma)$-model). Again, a spherical particle (see Fig. 1(c)) is discussed first (Sec. V), before the most general case of a freely rotating ellipsoidal particle (see Fig. 1(d)) is considered in Sec. VI.

III. SPHERICAL PARTICLE WITH ONE ORIENTATIONAL DEGREE OF FREEDOM

This section contains the theoretical considerations concerning the situation in Fig. 1(a) ($(D, 1, s)$-model). Although a spherical object is regarded here, one has to consider that a certain direction is specified through the theoretically assumed driving force $\mathbf{F} = F\hat{\mathbf{u}}$. The two-dimensional motion of the self-propelled particle can be described by the coordinates x and y of the center of mass position vector $\mathbf{r}(t) = (x, y)$ and the angle ϕ between $\hat{\mathbf{e}}_\mathbf{x}$

and $\hat{\mathbf{u}} = (\cos\phi, \sin\phi)$. Thus, the basic Langevin equations are given by

$$\frac{\mathrm{d}\mathbf{r}}{\mathrm{d}t} = \beta D_t \left[F\hat{\mathbf{u}} - \nabla U + \mathbf{f}\right] , \tag{1}$$

$$\frac{\mathrm{d}\phi}{\mathrm{d}t} = \beta D_r \mathbf{g}\cdot\hat{\mathbf{e}}_\mathbf{z} . \tag{2}$$

Here, $\mathbf{f}(t)$ and $\mathbf{g}(t)$ are the Gaussian white noise random force and torque, respectively. They are characterized by $\langle f_i(t)\rangle = 0$, $\langle f_i(t) f_j(t')\rangle = 2\delta_{ij}\delta(t-t')/(\beta^2 D_t)$, $\langle g_i(t)\rangle = 0$, and $\langle g_i(t) g_j(t')\rangle = 2\delta_{ij}\delta(t-t')/(\beta^2 D_r)$, where the indices i and j refer to the respective components, δ_{ij} is the Kronecker delta, and $\langle\ldots\rangle$ denotes a noise average. $U(\mathbf{r})$ is an external potential. The prefactors in Eqs. (1) and (2) consist of the inverse effective thermal energy $\beta = (k_\mathrm{B}T)^{-1}$ on the one hand and the translational and rotational short-time diffusion constants D_t and D_r on the other. In the case of a spherical particle with radius R these two quantities fulfill the relation $D_t/D_r = 4R^2/3$, which is used in the following analytical expressions for the displacement moments. The Langevin equation (2) can easily be derived from the more general vector equation $(\mathrm{d}\hat{\mathbf{u}})/(\mathrm{d}t) = \beta D_r \mathbf{g}(t)\times\hat{\mathbf{u}}$.

As ϕ is a linear combination of Gaussian variables according to Eq. (2), the respective probability distribution function has to be Gaussian as well and proves to be

$$P(\phi, t) = \frac{1}{\sqrt{4\pi D_\mathrm{r} t}} \exp\left(-\frac{(\phi-\phi_0)^2}{4D_\mathrm{r} t}\right) , \tag{3}$$

where $\phi_0 \equiv \phi(t=0)$ is the initial angle. For the theoretical analysis, the two-dimensional motion in the xy-plane can be split up into its components in x- and y-direction, respectively. In the following subsections, we first refer to the x-component of Eq. (1). As some calculations for the $(1,1,s)$-model have already been presented in [50] in more detail, we only summarize the most important results and briefly refer to systems with additional linear or quadratic potentials after that.

A. The $(1,1,s)$-model

Integrating the averaged Eq. (1) for $U = 0$ over time and considering only the x-component yields

$$\langle x(t) - x_0\rangle = \frac{4}{3}\beta F R^2 \cos(\phi_0)\left[1 - e^{-D_r t}\right] \tag{4}$$

and

$$\begin{aligned}\left\langle (x(t)-x_0)^2\right\rangle = {}& \frac{8}{3}R^2 D_r t + \left(\frac{4}{3}\beta F R^2\right)^2 \\ & \times\left[D_r t - 1 + e^{-D_r t} + \frac{1}{12}\cos(2\phi_0)\right. \\ & \left.\times\left(3 - 4e^{-D_r t} + e^{-4D_r t}\right)\right]\end{aligned} \tag{5}$$

for the mean position and the mean square displacement.

As usual the skewness S and the kurtosis γ are defined as

$$S = \frac{\left\langle (x - \langle x\rangle)^3\right\rangle}{\left\langle (x-\langle x\rangle)^2\right\rangle^{3/2}} \tag{6}$$

and

$$\gamma = \frac{\left\langle (x - \langle x\rangle)^4\right\rangle}{\left\langle (x-\langle x\rangle)^2\right\rangle^{2}} - 3 , \tag{7}$$

respectively. A non-Gaussian behavior is manifested in non-zero values for S and γ. Using the notation $F_s^* = \beta R F$ for spherical particles and a scaled time $\tau = D_r t$, the third and fourth moments are given by the analytical results

$$\begin{aligned}\left\langle \frac{(x(t)-x_0)^3}{R^3}\right\rangle = {}& \frac{32}{3}F_s^*\tau\cos(\phi_0)\left(1-e^{-\tau}\right) + \frac{64}{27}F_s^{*3}\left[\cos(\phi_0)\left(3\tau - \frac{45}{8} + \frac{5}{2}\tau e^{-\tau} + \frac{17}{3}e^{-\tau} - \frac{1}{24}e^{-4\tau}\right)\right. \\ & \left. + \cos(3\phi_0)\left(\frac{1}{24} - \frac{1}{16}e^{-\tau} + \frac{1}{40}e^{-4\tau} - \frac{1}{240}e^{-9\tau}\right)\right]\end{aligned} \tag{8}$$

and

$$\begin{aligned}\left\langle \frac{(x(t)-x_0)^4}{R^4}\right\rangle = {}& \frac{64}{3}\tau^2 + \frac{256}{9}F_s^{*2}\tau\left[e^{-\tau} + \tau - 1 + \frac{1}{12}\cos(2\phi_0)\left(e^{-4\tau} - 4e^{-\tau} + 3\right)\right] \\ & + \frac{256}{81}F_s^{*4}\left[3\tau^2 - \frac{45}{4}\tau + \frac{261}{16} - 5\tau e^{-\tau} - \frac{49}{3}e^{-\tau} + \frac{1}{48}e^{-4\tau}\right. \\ & + \cos(2\phi_0)\left(\frac{3}{2}\tau - \frac{19}{6} + \frac{5}{3}\tau e^{-\tau} + \frac{229}{72}e^{-\tau} - \frac{1}{30}\tau e^{-4\tau} - \frac{7}{450}e^{-4\tau} + \frac{1}{600}e^{-9\tau}\right) \\ & \left. + \cos(4\phi_0)\left(\frac{1}{192} - \frac{1}{120}e^{-\tau} + \frac{1}{240}e^{-4\tau} - \frac{1}{840}e^{-9\tau} + \frac{1}{6720}e^{-16\tau}\right)\right] .\end{aligned} \tag{9}$$

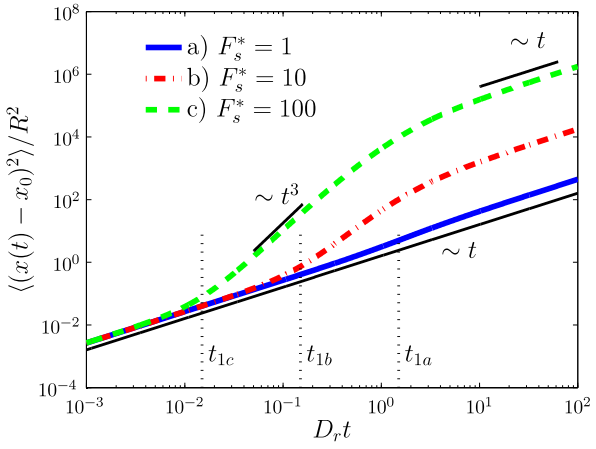

FIG. 2. (Color online) Mean square displacement of a spherical particle with initial orientation angle $\phi_0 = 0.5\pi$ for different values of $F_s^* = \beta RF$. The different time dependences in the various regimes are illustrated by straight lines.

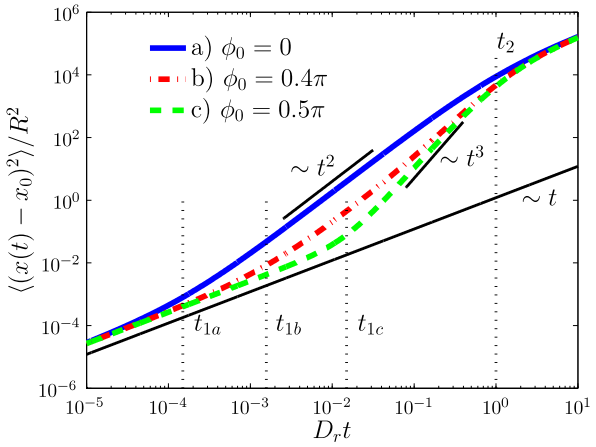

FIG. 3. (Color online) Mean square displacement of a spherical particle with effective force $F_s^* = 100$ for different values of ϕ_0. The regime of super-diffusive motion is defined by the time scales t_1 and t_2. While t_2 is independent of the initial angle ϕ_0, the time scale t_1 is the bigger the more the initial orientation of the particle deviates from the x-direction.

In the case of large forces $\beta RF \gg 1$, the particle motion (see Figs. 2 and 3) is separated into three qualitatively different time regimes, two diffusive regimes at short and at large times, and a super-diffusive regime at intermediate times, which is characterized by a t^2 or a t^3 behavior of the mean square displacement, depending on the initial particle orientation. These regimes are separated by the two time scales t_1 and t_2, respectively: At early times $t \ll t_1$, the particle undergoes simple translational Brownian motion, which is governed by the short time translational diffusion term $(8/3)R^2 D_r t$ in Eq. (5). As seen in Figs. 2 and 3 the mean square displacement displays a crossover to an intermediate super-diffusive regime at a time scale t_1, which, in turn, depends on the initial orientation ϕ_0 and the effective force $F_s^* = \beta RF$. In particular,

$$t_1 = \begin{cases} (3/2)(\beta RF D_r)^{-1}, & |\cos(\phi_0)| < 1/\sqrt{\beta RF} \\ (3/2)[\cos(\phi_0)\beta RF]^{-2} D_r^{-1}, & |\cos(\phi_0)| > 1/\sqrt{\beta RF} \end{cases}. \tag{10}$$

If the initial orientation has a sufficiently large component parallel to the x-axis, i.e., if $|\cos(\phi_0)| > 1/\sqrt{\beta RF}$, the mean square displacement displays a crossover to a ballistic regime, which is governed by a scaling relation $\langle (x(t) - x_0)^2 \rangle \propto t^2$. The crossover is observed the earlier the larger the inital force component $|\cos(\phi_0)|\beta RF$ parallel to the x-axis. On the contrary, if the initial particle orientation points along or almost along the y-axis at $t = 0$, i.e., $|\cos(\phi_0)| < 1/\sqrt{\beta RF}$, the crossover time t_1 is substantially larger. In the latter case t_1 is the time it takes the particle to undergo an angular displacement by rotational diffusion, such that the projected force onto the x-axis becomes as large as demanded in the former case. Only then does the force bring about a lateral displacement that is compatible or larger than the displacements due to original translational Brownian motion. Due to this multiplicative coupling of a diffusive and a ballistic behavior for the angular and the translational displacements, respectively, the mean square displacement shows a super-ballistic power-law behavior for $t \gg t_1$, with $\langle (x(t) - x_0)^2 \rangle \propto t^3$.

The intermediate regime is terminated by free rotational Brownian motion at the second time scale $t_2 = D_r^{-1}$, beyond which the particle motion is diffusive again. As already reported in Ref. [50], the long-time translational diffusion constant is given by

$$\begin{aligned} D_L &\equiv \lim_{t\to\infty} \frac{\langle (x(t) - x_0)^2 \rangle}{2t} \\ &= \frac{4}{3} D_r R^2 \left[1 + \frac{2}{3} (\beta RF)^2 \right]. \end{aligned} \tag{11}$$

As can be seen in Fig. 4, the beginning of the super-diffusive regime also shows up in the kurtosis. Here, the deviation from zero clearly indicates the crossover to non-Gaussian behavior. Interestingly, the kurtosis features a pronounced long-time tail. Therefore, the behavior of the particle is still non-Gaussian when its motion is (nearly) diffusive again. Analysing the analytical result for the kurtosis gives the leading long-time behavior as

$$\gamma(t) = \frac{-21 F_s^{*4}}{9 + 12\, F_s^{*2} + 4\, F_s^{*4}} (D_r t)^{-1} + \mathcal{O}\left(\frac{1}{t^2} \right). \tag{12}$$

As the amplitude vanishes for $F_s^* = 0$, this negative $1/t$ long-time tail in $\gamma(t)$ proves to be characteristic for self-propelled particles.

The previous calculation of the displacement moments can also be done for systems in which the self-propelled Brownian particle is exposed to x-dependent linear or quadratic potentials. This is illustrated in the following.

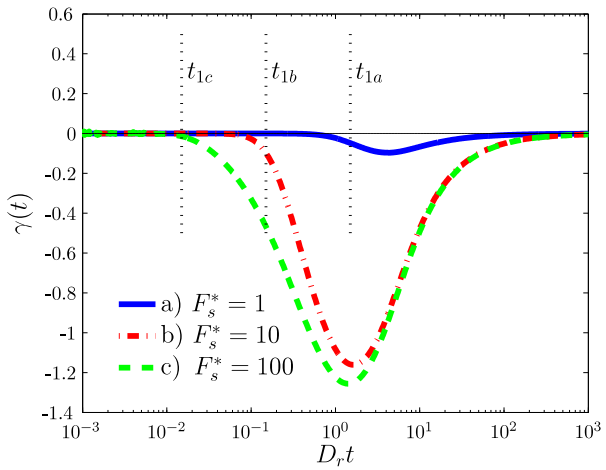

FIG. 4. (Color online) Kurtosis $\gamma(t)$ of the probability distribution function $\Psi(x,t)$ of a spherical particle with initial orientation angle $\phi_0 = 0.5\pi$ for the same values of $F_s^* = \beta RF$ as used in Fig. 2. Comparing Figs. 2 and 4 shows that the time scales t_{1a}, t_{1b} and t_{1c} can be extracted from the plots of the kurtosis as well as from the mean square displacement.

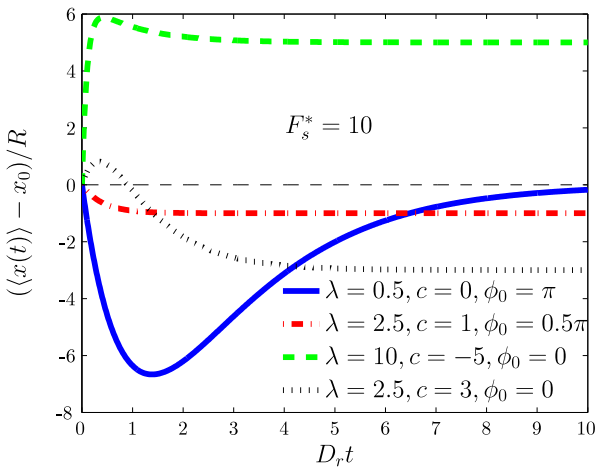

FIG. 5. (Color online) Mean position of a spherical particle with driving force $F_s^* = 10$ that is exposed to an external square potential. The strength of the potential $U(x) = (1/2)kx^2$ is determined by the parameter $\lambda = (4/3)\beta k R^2$. The dimensionless quantity $c = x_0/R$ is the distance between the initial position of the particle and the position of minimal potential given in units of particle radius R.

B. The $(1,1,s)$-model with an additional linear potential

The Langevin equations in this case are obtained from Eqs. (1) and (2) by simply inserting a linear potential of the form $U(x) = mgx$ into the first component of Eq. (1). Thus, the motion of a particle that is exposed to gravity is described by the moments

$$\langle x(t) - x_0\rangle = \frac{4}{3}\beta R^2 \left[F\cos(\phi_0)\left(1 - e^{-D_r t}\right) - mgD_r t\right] \tag{13}$$

and

$$\begin{aligned}\left\langle (x(t) - x_0)^2\right\rangle = {} & \frac{8}{3}R^2 D_r t + \left(\frac{4}{3}\beta R^2\right)^2 \Bigg\{ (mgD_r t)^2 \\ & + F^2\Bigg[D_r t - 1 + e^{-D_r t} + \frac{1}{12}\cos(2\phi_0) \\ & \times \left(3 - 4e^{-D_r t} + e^{-4D_r t}\right)\Bigg] \\ & - 2Fmg\cos(\phi_0) D_r t\left(1 - e^{-D_r t}\right)\Bigg\}.\end{aligned} \tag{14}$$

While the first moment (Eq. (13)) is a simple superposition of the terms due to the self-propulsion of the particle and the external force, respectively, the mean square displacement (Eq. (14)) has an additional term which depends on both of these forces.

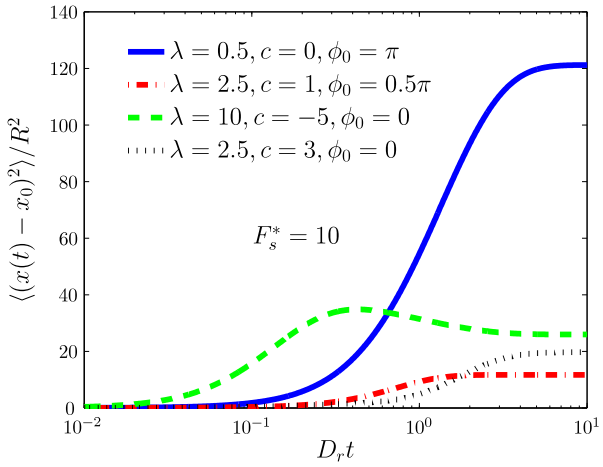

FIG. 6. (Color online) Mean square displacement of a spherical particle that is exposed to an external square potential. The plots refer to the same parameters as the plots in Fig. 5.

C. The $(1,1,s)$-model with an additional square potential

Based on the Langevin equations (1) and (2) one also obtains analytical results for the harmonic oscillator or square potential $U(x) = (1/2)kx^2$. Using the dimensionless parameter $\lambda = (4/3)\beta k R^2$, which determines the strength of the square potential, the mean position is given by

$$\langle x(t)\rangle = x_0 e^{-\lambda D_r t} + \frac{4\beta R^2 F}{3(\lambda - 1)}\cos(\phi_0)\left(e^{-D_r t} - e^{-\lambda D_r t}\right) \tag{15}$$

and the mean square displacement is calculated as

$$\begin{aligned}\langle (x(t)-x_0)^2\rangle = x_0^2\left(e^{-\lambda D_r t}-1\right)^2 + x_0\frac{8\beta R^2 F}{3(\lambda-1)}\cos(\phi_0)\left(e^{-\lambda D_r t}-1\right)\left(e^{-D_r t}-e^{-\lambda D_r t}\right) + \frac{4R^2}{3\lambda}\left(1-e^{-2\lambda D_r t}\right)\\ + \left(\frac{4}{3}\beta R^2 F\right)^2\left\{\frac{1}{(\lambda+1)}\left[\frac{1}{2\lambda}\left(1-e^{-2\lambda D_r t}\right)-\frac{1}{(\lambda-1)}\left(e^{-(\lambda+1)D_r t}-e^{-2\lambda D_r t}\right)\right]\right.\\ \left. + \frac{\cos(2\phi_0)}{(\lambda-3)}\left[\frac{1}{(2\lambda-4)}\left(e^{-4D_r t}-e^{-2\lambda D_r t}\right)-\frac{1}{(\lambda-1)}\left(e^{-(\lambda+1)D_r t}-e^{-2\lambda D_r t}\right)\right]\right\}.\end{aligned} \tag{16}$$

Figure 5 shows that the mean position of the particle reaches the position of the minimal potential and stays there. Due to the square potential, the mean square displacement (see Fig. 6) does not diverge as in the cases that have been regarded up to this point.

D. The $(2,1,s)$-model

In this section we briefly want to present the results for the $(2,1,s)$-model. As the one-dimensional case with the theoretically assumed internal force projected onto the x-axis was already considered in the preceding subsections, the analytical expressions for the first and second moments based on the two-dimensional Langevin equation (1) are given by superposition of the motion in x- and y-direction. Thus, using Eqs. (4) and (5) one obtains the vectorial mean position

$$\langle \mathbf{r}(t)-\mathbf{r}_0\rangle = \frac{4}{3}\beta F R^2\left[1-e^{-D_r t}\right]\begin{pmatrix}\cos(\phi_0)\\ \sin(\phi_0)\end{pmatrix} \tag{17}$$

and the mean square displacement

$$\begin{aligned}\left\langle (\mathbf{r}(t)-\mathbf{r}_0)^2\right\rangle = \frac{16}{3}R^2 D_r t\\ + 2\left(\frac{4}{3}\beta F R^2\right)^2\left[D_r t-1+e^{-D_r t}\right].\end{aligned} \tag{18}$$

As expected, the ϕ_0-dependence vanishes in Eq. (18) due to the free translational motion in the two-dimensional plane. Furthermore, the diffusive term given by the first summand in Eq. (18) is naturally twice as big as in Eq. (5).

IV. ELLIPSOIDAL PARTICLE WITH ONE ORIENTATIONAL DEGREE OF FREEDOM

We now generalize the previous considerations to ellipsoidal particles. To cover the situation depicted in Fig. 1(b) we have to take into account that, as opposed to the case of spherical particles, the translational diffusion coefficient is anisotropic, which means that the diffusion tensor

$$\mathbf{D_t} = D_a(\hat{\mathbf{u}}\otimes\hat{\mathbf{u}}) + D_b(\mathbf{I}-\hat{\mathbf{u}}\otimes\hat{\mathbf{u}}) \tag{19}$$

has to be applied. Here, $\mathbf{I}$ is the 2×2 unit matrix, $\hat{\mathbf{u}} = (\cos\phi, \sin\phi)$ is the orientation vector, $\otimes$ a dyadic product, and D_a and D_b, respectively, indicate the diffusion coefficients for translation in the direction of the two semi-axes of the ellipsoid. The index a stands for the semi-major axis, while b marks the semi-minor axis. Using the diffusion tensor (Eq. (19)), the Langevin equation for the center of mass position of the particle can be written in the form

$$\frac{\mathrm{d}\mathbf{r}}{\mathrm{d}t} = \beta\mathbf{D_t}\cdot[F\hat{\mathbf{u}}-\nabla U] + \mathbf{w}\,. \tag{20}$$

Due to the anisotropy of the diffusion coefficient we cannot include the Gaussian white noise random force exactly in the same way as in Eq. (1). Instead of that, we use the zero mean random noise source $\mathbf{w}(t)$. The variances of the components $i,j\in\{x,y\}$ are given by $\langle w_i(t)w_j(t')\rangle = 2D_t^{ij}(\phi(t))\delta(t-t')$. Thus, $w_i(t)$ are Gaussian random variables at fixed $\phi(t)$. This follows the procedure presented in Ref. [37] for "passive" ellipsoidal particles.

A. The $(1,1,e)$-model

It can easily be seen from Eq. (19) that $\mathbf{D_t}\cdot\hat{\mathbf{u}} = D_a\hat{\mathbf{u}}$. Therefore, in the context of the $(1,1,e)$-model the Langevin equation for the center of mass position x of the self-propelled particle without external potentials can be written as

$$\frac{\mathrm{d}x}{\mathrm{d}t} = \beta D_a F\cos(\phi) + w_x\,. \tag{21}$$

The Langevin equation for the angle ϕ, which is needed in addition to Eq. (21), does not differ from Eq. (2). For the following calculations, it is convenient to write the

diffusion tensor (Eq. (19)) as

$$\mathbf{D_t} = \overline{D}\mathbf{I} + \frac{1}{2}\Delta D \begin{pmatrix} \cos(2\phi) & \sin(2\phi) \\ \sin(2\phi) & -\cos(2\phi) \end{pmatrix}, \tag{22}$$

where $\overline{D} = 1/2(D_a + D_b)$ marks the mean diffusion coefficient and ΔD the difference $D_a - D_b$ between the diffusion coefficients along the long and short axes of the ellipsoid.

The mean position of an ellipsoidal particle is given by the first component of Eq. (24). For the mean square displacement one obtains the relation

$$\begin{aligned} \left\langle (x(t) - x_0)^2 \right\rangle = 2\overline{D}t + \frac{\Delta D}{4D_r}\cos(2\phi_0)\left(1 - e^{-4D_r t}\right) \\ + \left(\beta F \frac{D_a}{D_r}\right)^2 \Big[D_r t - 1 + e^{-D_r t} \\ + \frac{1}{12}\cos(2\phi_0)\left(3 - 4e^{-D_r t} + e^{-4D_r t}\right)\Big]. \end{aligned} \tag{23}$$

For an isotropic particle with $\Delta D = 0$ Eq. (23) reduces to the result for a spherical particle in one dimension (Eq. (5)), as expected. For an anisotropic particle the additional (second) term in Eq. (23) yields a ϕ_0-dependence at very early times, in the regime of bare translational diffusion, which is not present in the case of an isotropic particle (see the discussion in Sec. III A). This additional term represents the relative orientation of the initial direction of the long axis of the ellipsoidal particle and the direction of the linear channel. The ϕ_0-dependence can also be seen in Fig. 7, where the strength of the driving force is determined by the parameter $F_e^* = \beta F_0 \sqrt{D_a/D_r}$ for ellipsoidal particles.

The analytical results for the third and fourth moments, which are needed to calculate skewness and kurtosis, are more complicated and, therefore, given in the appendix in Eqs. (A.1) and (A.2), respectively.

B. The $(2, 1, e)$-model

Again, we provide the analytical results for the case with two-dimensional translation as well. For an ellipsoidal particle, one obtains the expressions

$$\langle \mathbf{r}(t) - \mathbf{r}_0 \rangle = \beta F \frac{D_a}{D_r}\left[1 - e^{-D_r t}\right]\begin{pmatrix}\cos(\phi_0)\\ \sin(\phi_0)\end{pmatrix} \tag{24}$$

for the first moment and

$$\left\langle (\mathbf{r}(t) - \mathbf{r}_0)^2 \right\rangle = 4\overline{D}t + 2\left(\beta F \frac{D_a}{D_r}\right)^2 \left[D_r t - 1 + e^{-D_r t}\right] \tag{25}$$

for the mean square displacement, respectively. As in the mean square displacement of a spherical particle (Eq. (18)), the ϕ_0-dependence also vanishes in Eq. (25). Furthermore, the contribution to the diffusive motion due to the initial orientation of the particle disappears for two-dimensional translation so that the diffusive motion is simply reflected by the term $4\overline{D}t$ in Eq. (25).

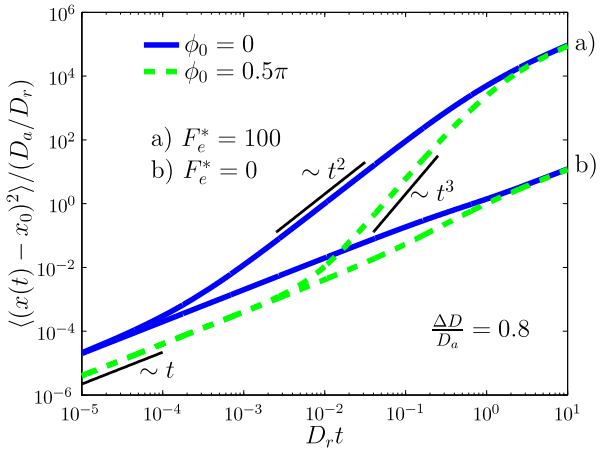

FIG. 7. (Color online) Mean square displacement of an ellipsoidal particle with one orientational degree of freedom and anisotropy $\Delta D/D_a = 0.8$. Plots are shown for a) a self-propelled particle with $F_e^* = \beta F_0 \sqrt{D_a/D_r} = 100$ and b) a "passive" particle with vanishing effective force. The solid lines refer to a parallel and the dashed lines to a perpendicular initial orientation.

V. FREELY ROTATING SPHERICAL PARTICLE

Up to now, particles with only one orientational degree of freedom have been examined. In this section we transfer our model to particles whose orientation is freely diffusing on the unit sphere. Considering a spherical particle this situation is shown in Fig. 1(c). In the Cartesian lab frame the particle orientation $\hat{\mathbf{u}} = (\sin\theta\cos\varphi, \sin\theta\sin\varphi, \cos\theta)$ is now given in terms of the two orientation angles θ and φ. Using the updated orientation vector the Langevin equation for the center of mass position is identical to Eq. (1) if the third component of all vectorial quantities is considered additionally.

The orientational probability distribution for the freely diffusing orientation vector [45] is given by

$$P(\theta, \varphi, t) = \sum_{l=0}^{\infty}\sum_{m=-l}^{l} e^{-D_r l(l+1)t}\, Y_l^{m*}(\theta_0, \varphi_0) Y_l^m(\theta, \varphi), \tag{26}$$

where Y_l^m are the spherical harmonics. In Eq. (26) we use the notation $\theta_0 \equiv \theta(t = 0)$ and $\varphi_0 \equiv \varphi(t = 0)$ while the star indicates complex conjugation.

A. The $(1, 2, s)$-model

To eliminate the φ-dependence in the equation of motion, we choose the z-axis to point in the direction of the linear channel, which we consider first. Moreover, we omit external potentials in the following. By calculating

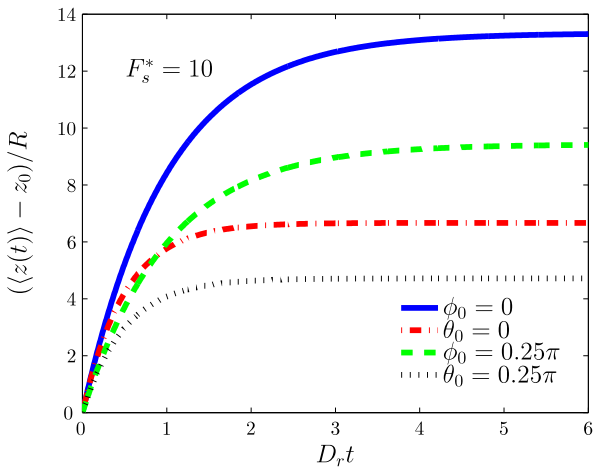

FIG. 8. (Color online) Comparison of the mean position of a spherical particle with one and with two orientational degrees of freedom. The graphs for which the initial angle ϕ_0 is given refer to the $(1,1,s)$-model while the graphs designated by a certain value for the angle θ_0 show the results for the $(1,2,s)$-model. In all cases the effective force is $F_s^* = 10$ and the motion in z-direction is considered.

$\langle \cos(\theta) \rangle$ via Eq. (26) the first moment is obtained as

$$\langle z(t) - z_0 \rangle = \frac{2}{3} \beta F R^2 \cos(\theta_0)(1 - e^{-2D_r t}) \,. \tag{27}$$

The mean position in the $(1,2,s)$-model is very similar to the same in the $(1,1,s)$-model (see Eq. 4). Here, the azimuthal angle θ takes the role of the angle ϕ in the $(1,1,s)$-model. In particular, the two results agree up to linear order in time t, whereas they deviate for longer times due to the enhanced probability of the sphere with full orientational freedom to assume a configuration with an orientation pointing in the direction of the equator. This, in turn, on average causes a smaller force component along the z-axis and a smaller plateau-value of the excursion $\lim_{t\to\infty} \langle z(t) - z(0) \rangle$, which is illustrated in Fig. 8.

Using Eq. (26) and, thus, the fact that every function that depends exclusively on θ and φ can be expanded as a linear combination of spherical harmonics, we also obtain the analytical result for the mean square displacement, which is given by

$$\begin{aligned} \langle (z(t) - z_0)^2 \rangle = {} & \frac{8}{3} R^2 D_r t + \left(\frac{2}{9} \beta F R^2 \right)^2 \\ & \times \Big[12 D_r t - 8 + 9 e^{-2D_r t} - e^{-6D_r t} \\ & + \cos^2(\theta_0) \left(6 - 9 e^{-2D_r t} + 3 e^{-6D_r t} \right) \Big] \,. \end{aligned} \tag{28}$$

Comparing Eqs. (28) and (5) (as shown in Fig. 9) it turns out that also the mean square displacements of the spheres with two or one orientational degree of freedom in a linear channel are almost identical. In particular,

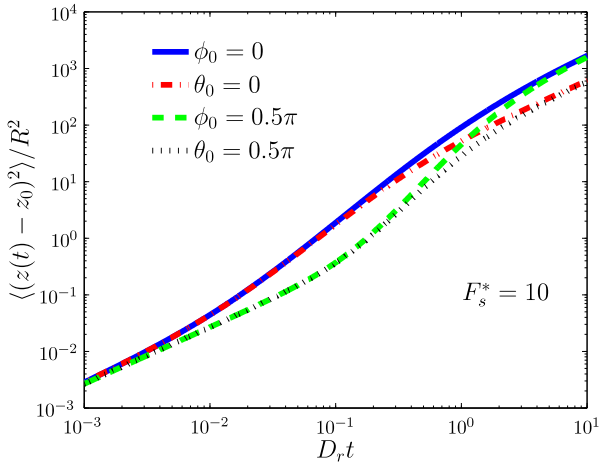

FIG. 9. (Color online) Comparison of the mean square displacement of a spherical particle with one and with two orientational degrees of freedom. The remarks in the caption of Fig. 8 are also valid for this figure.

their functional forms are the same up to second or third order in time t, for the cases of a parallel ($\phi_0 = \theta_0 \approx 0$) or a perpendicular ($\phi_0 = \theta_0 \approx \pi/2$) initial configuration, respectively. Therefore, the crossover time scale from the diffusive to the super-diffusive regime t_1 is exactly the same as in the $(1,1,s)$-model and given by Eq. (10). The second time scale from the super-diffusive to the diffusive regime is in the $(1,2,s)$-model given by $t_2 = (2D_r)^{-1}$ and therefore half as large as in the $(1,1,s)$-model. Concomitantly, the long-time diffusion constant is smaller as compared to Eq. (11) and given by

$$D_L = \frac{4}{3} D_r R^2 \left[1 + \frac{2}{9} (\beta R F)^2 \right] \,. \tag{29}$$

As for the long-time limits of the mean positions, the difference to Eq. (11) reflects the fact that the freely oriented sphere is more likely oriented perpendicular to the channel axis than the sphere that is confined to rotate in the plane.

The non-Gaussian behavior of the self-propelled particle with free orientation on the unit sphere is embodied in the third moment

$$\left\langle \frac{(x(t)-x_0)^3}{R^3} \right\rangle = 16/3\, F_s^*\, \tau\, \cos(\theta)(1-e^{-2\,\tau}) + \frac{64}{27}\, F_s^{*3}\Big[-\frac{41}{96}\,\cos(\theta) + \frac{1}{96}\,\cos(3\,\theta) + \frac{351}{800}\,\cos(\theta)e^{-2\,\tau} - \frac{3}{160}\,\cos(3\,\theta)e^{-2\,\tau} + 1/2\,\cos(\theta)\tau - \frac{1}{800}\,\cos(\theta)e^{-12\,\tau} - \frac{1}{96}\,\cos(\theta)e^{-6\,\tau} + \frac{1}{96}\,\cos(3\,\theta)e^{-6\,\tau} + 3/10\,\cos(\theta)\tau\, e^{-2\,\tau} - \frac{1}{480}\,e^{-12\,\tau}\cos(3\,\theta)\Big] \tag{30}$$

and in the fourth moment

$$\left\langle \frac{(x(t)-x_0)^4}{R^4} \right\rangle = \frac{64}{3}\,\tau^2 + \frac{64}{81}\,F_s^{*2}\tau\left[12\,\tau - 8 + 9\,e^{-2\,\tau} - e^{-6\,\tau} + (\cos(\theta))^2\left(6 - 9\,e^{-2\,\tau} + 3\,e^{-6\,\tau}\right)\right] + \frac{2}{893025}\,F_s^{*4}\Big[27\,e^{-20\,\tau} + 588\,\cos(2\,\theta)e^{-12\,\tau} - 16800\,\tau\,\cos(2\,\theta)e^{-6\,\tau} - 735\,\cos(4\,\theta)e^{-12\,\tau} + 470400\,\tau^2 + 147\,e^{-12\,\tau} + 1100\,e^{-6\,\tau} - 5600\,\tau\,e^{-6\,\tau} + 480298 - 481572\,e^{-2\,\tau} - 211680\,\tau\,e^{-2\,\tau} + 105\,e^{-20\,\tau}\cos(4\,\theta) + 60\,e^{-20\,\tau}\cos(2\,\theta) + 1470\,\cos(4\,\theta) - 237160\,\cos(2\,\theta) - 736960\,\tau - 2940\,\cos(4\,\theta)e^{-2\,\tau} + 249312\,\cos(2\,\theta)e^{-2\,\tau} + 211680\,\tau\,\cos(2\,\theta)e^{-2\,\tau} + 235200\,\tau\,\cos(2\,\theta) + 2100\,\cos(4\,\theta)e^{-6\,\tau} - 12800\,\cos(2\,\theta)e^{-6\,\tau}\Big]. \tag{31}$$

The curves for the skewness (see Fig. 10) and the kurtosis (see Fig. 11) of the probability distribution function $\Psi(x,t)$ for the $(1,2,s)$-model are obtained by shrinking their counterparts for the $(1,1,s)$-model in x-direction as well as in the direction of the t-axis. This is very similar to the findings concerning the mean position of the particle (see Fig. 8). The extrema of skewness and kurtosis and the change of sign of the kurtosis, that is observed for non-perpendicular initial configurations, already occur at smaller times. Obviously, the existence of the negative $1/t$ long-time tail in $\gamma(t)$ (see Sec. III A) is not affected by the number of orientational degrees of freedom of the particle.

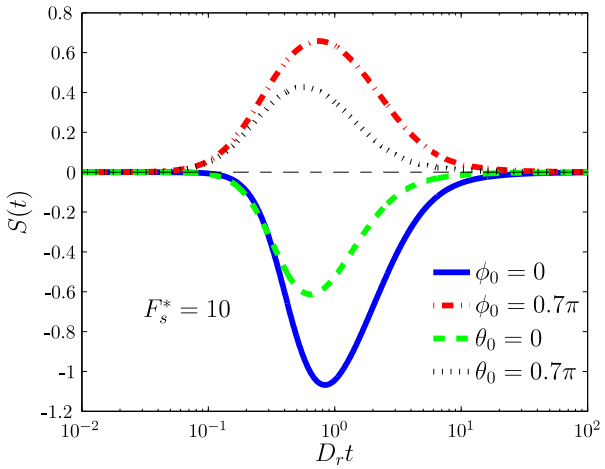

FIG. 10. (Color online) Comparison of the skewness $S(t)$ of the probability distribution function $\Psi(x,t)$ for a spherical particle with one and with two orientational degrees of freedom. The solid and the dash-dotted lines refer to the $(1,1,s)$-model while their counterparts for the $(1,2,s)$-model are given by the dashed and the dotted lines.

B. The $(2,2,s)$-model

For more than one translational degree of freedom, if the particle motion takes place in the xy-plane, the first and second moments are given by

$$\langle \mathbf{r}(t) - \mathbf{r}_0 \rangle = \frac{2}{3}\beta F R^2 \left(1 - e^{-2D_r t}\right) \begin{pmatrix} \sin(\theta_0)\cos(\varphi_0) \\ \sin(\theta_0)\sin(\varphi_0) \end{pmatrix} \tag{32}$$

and

$$\langle (\mathbf{r}(t) - \mathbf{r}_0)^2 \rangle = \frac{16}{3} R^2 D_r t + \left(\frac{2}{9}\beta F R^2\right)^2 \times \Big[24 D_r t - 16 + 18 e^{-2D_r t} - 2e^{-6D_r t} + \sin^2(\theta_0)(6 - 9e^{-2D_r t} + 3e^{-6D_r t})\Big], \tag{33}$$

respectively. As before, the results for the mean position and the mean square displacement are almost identical with respect to their lower-dimensional counterparts. Beside the change from a cosine to a sine in the last part of Eq. (33), which is due to the change of accessible dimensions, the only difference of the mean square displacements in the $(2,2,s)$- and in the $(1,2,s)$-model consists in an additional factor of 2 for all terms that do not depend on θ_0.

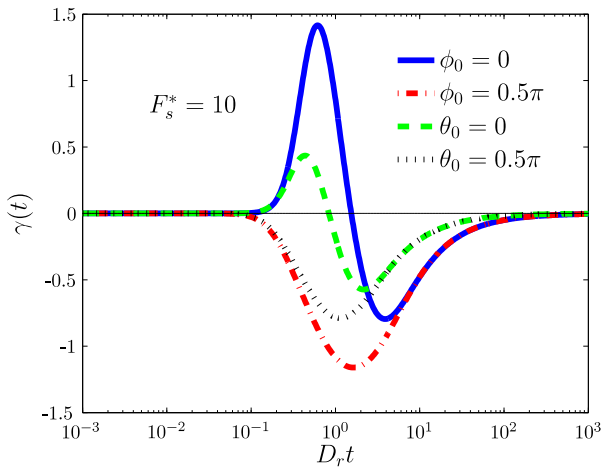

FIG. 11. (Color online) Comparison of the kurtosis $\gamma(t)$ of $\Psi(x,t)$ for a spherical particle with one and with two orientational degrees of freedom. See also the remarks in the caption of Fig. 10.

C. The $(3,2,s)$-model

The $(3,2,s)$-model is the most general situation concerning a spherical particle. In this case, the mean position of the particle is obtained by adding the z-component (Eq. (27)) to Eq. (32). The mean square displacement is given by

$$\langle(\mathbf{r}(t)-\mathbf{r}_0)^2\rangle = 8R^2D_r t + \frac{1}{2}\left(\frac{4}{3}\beta F R^2\right)^2\left[2D_r t - 1 + e^{-2D_r t}\right]. \tag{34}$$

The simplicity of Eq. (34) can be explained by the fact that no dependence on the initial orientation can appear due to the completely free motion [53].

VI. FREELY ROTATING ELLIPSOIDAL PARTICLE

To complete our examination of the different model situations, we now consider a freely rotating self-propelled ellipsoidal particle as sketched in Fig. 1(d). The $(D,2,e)$-models, where $D \in \{1,2,3\}$ is the number of translational degrees of freedom, are based on the Langevin equation (20). To transfer this two-dimensional equation to the three-dimensional case regarded here, the orientation vector $\hat{\mathbf{u}} = (\sin\theta\cos\varphi, \sin\theta\sin\varphi, \cos\theta)$ is used and the third component is added to all vectorial quantities. The explicit form of the diffusion tensor $\mathbf{D_t}$ is given by Eq. (19) by means of the updated orientation vector.

A. The $(1,2,e)$-model

As in the previous sections, we begin by considering the case of one-dimensional translational motion without external potentials, i.e., with the $(1,2,e)$-model. Using the ansatz based on spherical harmonics according to Eq. (26) for an ellipsoidal particle leads to the analytical results

$$\langle z(t) - z_0\rangle = \frac{1}{2}\beta F\frac{D_a}{D_r}\left[1 - e^{-2D_r t}\right]\cos(\theta_0) \tag{35}$$

for the mean position and

$$\begin{aligned}\langle(z(t)-z_0)^2\rangle = {} & 2\overline{D}t + \left(\frac{1}{6}\beta F\frac{D_a}{D_r}\right)^2 \\ & \times\Big[12D_r t - 8 + 9e^{-2D_r t} - e^{-6D_r t} \\ & \quad + \cos^2(\theta_0)\left(6 - 9e^{-2D_r t} + 3e^{-6D_r t}\right)\Big] \\ & + \frac{\Delta D}{9D_r}\Big[-3D_r t - 1 + e^{-6D_r t} \\ & \quad + 3\cos^2(\theta_0)\left(1 - e^{-6D_r t}\right)\Big]\end{aligned} \tag{36}$$

for the mean square displacement, respectively. Corresponding expressions for the third and fourth moments and, thus, for skewness and kurtosis were calculated as well. As these are quite lengthy, they are given in the appendix in Eqs. (A.3) and (A.4), respectively, but are presented graphically in Figs. 12 and 13. Different regimes of non-Gaussian behavior are manifested by different signs of the kurtosis. For "passive" particles with vanishing internal effecitve force $F_e^* = 0$ (solid line in Fig. 13) no change of sign is observed. The kurtosis is positive and a simple maximum occurs at $t \approx t_2 = (2D_r)^{-1}$. These findings correspond to the results for "passive" ellipsoidal particles in two dimensions that were studied in Ref. [37]. In contrast to simple non-Gaussian behaviour, the situation turns out to be much more complex if self-propelled particles are considered. If the self-propulsion outweighs the effect of the kicks of the solvent particles (dashed line and dotted line in Fig. 13), several maxima, minima, and changes of sign induce a rich structure in $\gamma(t)$ indicating different non-Gaussian behavior at different time scales. The characteristic $1/t$ long-time tail observed for spherical particles is also found for ellipsoidal self-propelled particles. The skewness $S(t)$ (see Fig. 12), which is a measure of the asymmetry of the probability distribution, reveals a higher degree of complexity as well. While $S(t)$ is zero for "passive" particles (solid line in Fig. 12), this parameter also shows a much richer structure if self-propelled particles are regarded.

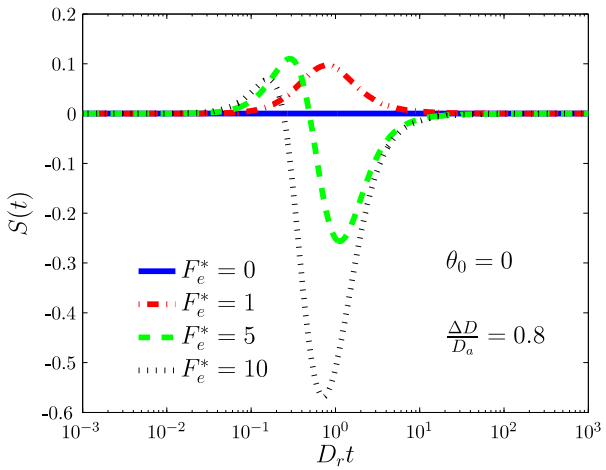

FIG. 12. (Color online) Skewness $S(t)$ of the probability distribution function $\Psi(x,t)$ for an ellipsoidal self-propelled particle as a function of time. This figure illustrates the analytical results of the $(1,2,e)$-model. While the initial angle θ_0 and the anisotropy $\Delta D/D_a$ are constant as given in the figure, graphs for various values of the effective force F_e^* are shown.

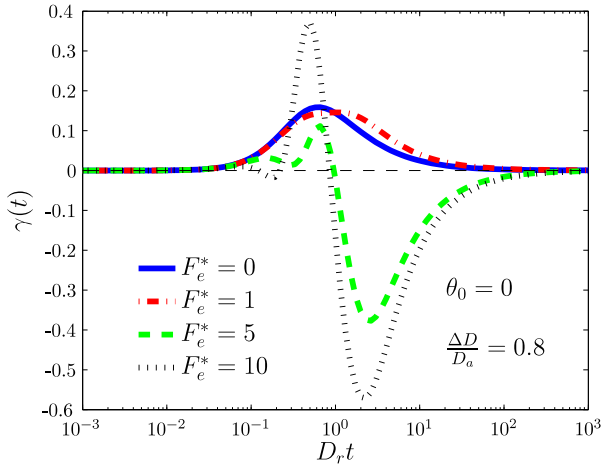

FIG. 13. (Color online) Kurtosis $\gamma(t)$ of $\Psi(x,t)$ for an ellipsoidal self-propelled particle as a function of time. The graphs correspond to the graphs in Fig. 12 as far as the values of the various parameters are concerned.

B. The $(2,2,e)$-model

By simply combining the results for one-dimensional translation in x- and in y-direction, for the $(2,2,e)$-model we obtain the expressions

$$\langle \mathbf{r}(t) - \mathbf{r}_0 \rangle = \frac{1}{2}\beta F \frac{D_a}{D_r}\left[1 - e^{-2D_r t}\right] \begin{pmatrix} \sin(\theta_0)\cos(\varphi_0) \\ \sin(\theta_0)\sin(\varphi_0) \end{pmatrix} \tag{37}$$

for the mean position and

$$\begin{aligned} \langle (\mathbf{r}(t) - \mathbf{r}_0)^2 \rangle = {} & 4\overline{D}t + \left(\frac{1}{6}\beta F \frac{D_a}{D_r}\right)^2 \\ & \times \Big[24 D_r t - 16 + 18 e^{-2D_r t} - 2 e^{-6D_r t} \\ & + \sin^2(\theta_0)\left(6 - 9e^{-2D_r t} + 3e^{-6D_r t}\right)\Big] \\ & + \frac{\Delta D}{9 D_r}\Big[-6D_r t - 2 + 2e^{-6D_r t} \\ & + 3\sin^2(\theta_0)\left(1 - e^{-6D_r t}\right)\Big] \end{aligned} \tag{38}$$

for the mean square displacement.

C. The $(3,2,e)$-model

In a last step, we now add the third translational degree of freedom. Hence, in this subsection we consider the most general case with free translational and rotational motion of an ellipsoidal self-propelled particle. By adding the third component (Eq. (35)) to Eq. (37) we obtain the result for the mean position. The analytical expression for the mean square displacement is simply given by

$$\begin{aligned} \langle (\mathbf{r}(t) - \mathbf{r}_0)^2 \rangle = {} & 6\overline{D}t - \Delta D t \\ & + \frac{1}{2}\left(\beta F \frac{D_a}{D_r}\right)^2 \left[2D_r t - 1 + e^{-2D_r t}\right] . \end{aligned} \tag{39}$$

To explain the simplicity of this result we want to point to the short discussion after Eq. (34).

VII. CONCLUSION

In conclusion, we have analytically solved the Brownian dynamics of an anisotropic self-propelled particle in different geometries by presenting explicit results for the first four moments of the probability distribution function for displacements. The particle is driven along an axis which itself fluctuates according to rotational Brownian dynamics. After a transient regime which is characterized by two distinct time scales, there is diffusive behavior for long times. The results for the long-time diffusion constants D_L for the different groups of model situations are given in Table I. For intermediate times, non-Gaussian behavior is revealed by a non-vanishing kurtosis in the particle displacement which decays as $1/t$ for long times t. For special initial conditions (nearly perpendicular initial orientation and large effective forces), we find a superdiffusive transient regime where the mean square displacement scales with an exponent 3 in time. The analytical results can be used to compare with experimental

TABLE I. Long-time diffusion constant D_L for the different model situations. Using the definition in Eq. (11) the analytical results are directly obtained from the respective results for the mean square displacement.

Model	Long-time diffusion constant
$(D,1,s)$	$(4/3)D_rR^2\left[1+(2/3)(\beta FR)^2\right]$
$(D,1,e)$	$\overline{D}+1/(2D_r)\left(\beta F\left(\overline{D}+(1/2)\Delta D\right)\right)^2$
$(D,2,s)$	$(4/3)D_rR^2\left[1+(2/9)(\beta FR)^2\right]$
$(D,2,e)$	$\overline{D}-(1/6)\Delta D+1/(6D_r)\left(\beta F\left(\overline{D}+(1/2)\Delta D\right)\right)^2$

systems of, e.g., swimming bacteria or self-propelled colloidal particles. Any deviations point to the importance of hydrodynamic interactions with the substrate and with neighbouring particles at finite density.

It would be interesting to generalize the analysis towards various situations. First of all, hydrodynamic interactions were neglected in our studies. While this is justified in the bulk, hydrodynamic interactions become important at finite densities [54] and may significantly influence the distribution of the mean square displacements [55]. If the particle is moving close to a substrate and the substrate is hydrodynamically not flat, then hydrodynamic interactions play a significant role, too [56]. Second, it would be interesting to include an additional torque in the Langevin equations of motion. This leads to circular motion in two dimensions [32] while for three spatial dimensions helical motion is expected as also suggested by a slightly different model presented in Ref. [57]. Next, a non-Gaussian noise [58] in the Langevin equations might be relevant for modeling real swimming objects [13, 57]. Furthermore, the actual propulsion mechanism was modelled just by an effective force. A consideration of more details about the actual propulsion mechanism might be necessary to analyse short-time dynamics in more depth. In addition to that, the model migth be transferred to more complicated geometries [59] such as ratchets [9, 60, 61], for example. Finally, the collective dynamics [62–64] of many swimmers will lead to further effects like swarming, swirling and jamming. While at high densities hydrodynamic interactions are expected to play a minor role, the direct particle-particle interactions get relevant and should be incorporated in theory [65] and simulation [66].

ACKNOWLEDGMENTS

We thank T. Lubensky, H. H. Wensink, J. K. G. Dhont, J. Dunkel, and J. Yeomans for helpful discussions. This work was supported by the DFG (SFB TR6 - C3).

Appendix: Further analytical results

In the following, we summarize the analytical results for the third and fourth moments of an ellipsoidal particle. For reasons of clarity, we use the notation $F_e^*=\beta F_0\sqrt{D_a/D_r}$, the ratio $\delta=\Delta D/D_a$ and the scaled time $\tau=D_rt$. For the $(1,1,e)$-model the third moment is given by

$$\begin{aligned}\left\langle\frac{(x(t)-x_0)^3}{(D_a/D_r)^{3/2}}\right\rangle = F_e^{*3}\Big[&-\frac{45}{8}\cos(\phi)+\frac{1}{24}\cos(3\,\phi)+\frac{17}{3}\cos(\phi)e^{-\tau}-\frac{1}{16}\cos(3\,\phi)e^{-\tau}+3\cos(\phi)\tau-\frac{1}{24}\cos(\phi)e^{-4\,\tau}\\&+\frac{1}{40}\cos(3\,\phi)e^{-4\,\tau}+\frac{5}{2}\cos(\phi)\tau\,e^{-\tau}-\frac{1}{240}\,e^{-9\,\tau}\cos(3\,\phi)\Big]\\&+6\,F_e^*\left(1-\frac{1}{2}\,\delta\right)\Big[\cos(\phi)\tau-\cos(\phi)\tau\,e^{-\tau}\Big]\\&+3\,F_e^*\,\delta\Big[\frac{5}{8}\cos(\phi)+\frac{5}{72}\cos(3\,\phi)-\frac{2}{3}\cos(\phi)e^{-\tau}-\frac{1}{16}\cos(3\,\phi)e^{-\tau}\\&+\frac{13}{720}\,e^{-9\,\tau}\cos(3\,\phi)-\frac{1}{2}\cos(\phi)\tau\,e^{-\tau}+\frac{1}{24}\cos(\phi)e^{-4\,\tau}-\frac{1}{40}\cos(3\,\phi)e^{-4\,\tau}\Big]\end{aligned}\tag{A.1}$$

and the fourth moment is

$$\left\langle \frac{(x(t)-x_0)^4}{(D_a/D_r)^2} \right\rangle = \frac{1}{100800}\, F_e^{*4}\Big[15\, e^{-16\,\tau}\cos(4\,\phi) - 504000\,\tau\, e^{-\tau} - 1134000\,\tau + 1644300 + 168\,\cos(2\,\phi)e^{-9\,\tau} \\ - 319200\,\cos(2\,\phi) + 420\,\cos(4\,\phi)e^{-4\,\tau} + 525\,\cos(4\,\phi) + 2100\,e^{-4\,\tau} - 1646400\,e^{-\tau} \\ - 1568\,\cos(2\,\phi)e^{-4\,\tau} - 840\,\cos(4\,\phi)e^{-\tau} + 151200\,\tau\,\cos(2\,\phi) - 3360\,\tau\,\cos(2\,\phi)e^{-4\,\tau} \\ + 320600\,\cos(2\,\phi)e^{-\tau} - 120\,\cos(4\,\phi)e^{-9\,\tau} + 168000\,\tau\,\cos(2\,\phi)e^{-\tau} + 302400\,\tau^2\Big] \\ + F_e^{*2}\,(1-1/2\,\delta)\left[3\,\tau\,\cos(2\,\phi) - 12\,\tau - 4\,\tau\,\cos(2\,\phi)e^{-\tau} + 12\,\tau\,e^{-\tau} + \tau\,\cos(2\,\phi)e^{-4\,\tau} + 12\,\tau^2\right] \\ + 6\,F_e^{*2}\delta\left[\frac{6917529027641081855}{9223372036854775808}\,\tau + \frac{76861433640456465}{4611686018427387904}\,\tau\,\cos(2\,\phi)e^{-4\,\tau} - 1/6\,\tau\,\cos(2\,\phi)e^{-\tau}\right. \\ + \frac{9223372036854775807}{6917529027641081856}\,e^{-\tau} + \frac{461168601842738791}{332041393326771929088}\,\cos(4\,\phi)e^{-4\,\tau} \\ - \frac{2305843092136939525}{166020696663385964544}\,\cos(2\,\phi) - \frac{230584300921369395 1}{110680464442257309696}\,e^{-4\,\tau} \\ - \frac{39199331156632797169}{46485795065748070072320}\,e^{-16\,\tau}\cos(4\,\phi) - \frac{374699488997225267}{103762935414616227840}\,\cos(2\,\phi)e^{-9\,\tau} \\ - \frac{2767011611056432759}{830103483316929822720}\,\cos(2\,\phi)e^{-4\,\tau} + 1/4\,\tau\,\cos(2\,\phi) - \frac{11}{720}\,\cos(4\,\phi)e^{-\tau} \\ - \frac{4842270319348757 2987}{36893488147419103232} + \frac{374699488997225267}{145268109580462718976}\,\cos(4\,\phi)e^{-9\,\tau} \\ \left. + \frac{3026418949592973313}{20752587082923245568}\,\cos(2\,\phi)e^{-\tau} + 1/2\,\tau\,e^{-\tau} + \frac{161409010644958576 63}{132816557330708771 6352}\,\cos(4\,\phi)\right] \\ + 12\,(1-1/2\,\delta)^2\,\tau^2 + 3\,\delta\,(1-1/2\,\delta)\cos(2\,\phi)\tau\,\left(1-e^{-4\,\tau}\right) \\ + 3/4\,\delta^2\left[\tau - 1/4 + 1/4\,e^{-4\,\tau} + 1/48\,\cos(4\,\phi)(3-4\,e^{-4\,\tau}+e^{-16\,\tau})\right]\,. \qquad \text{(A.2)}$$

The corresponding results for a freely rotating ellipsoidal particle ($(1,2,e)$-model) are the third moment

$$\left\langle \frac{(x(t)-x_0)^3}{(D_a/D_r)^{3/2}} \right\rangle = \frac{1}{2400}\, F_e^{*3}\Big[-1025\,\cos(\theta) + 25\,\cos(3\,\theta) + 1053\,\cos(\theta)e^{-2\,\tau} - 45\,\cos(3\,\theta)e^{-2\,\tau} + 1200\,\cos(\theta)\tau \\ - 3\cos(\theta)e^{-12\tau} - 25\cos(\theta)e^{-6\tau} + 25\cos(3\theta)e^{-6\tau} + 720\cos(\theta)\tau e^{-2\tau} - 5e^{-12\tau}\cos(3\theta)\Big] \\ + 6\,F_e^{*}\,(1-1/2\,\delta)\left[1/2\,\cos(\theta)\tau - 1/2\,\cos(\theta)\tau\,e^{-2\,\tau}\right] \\ + 3F_e^{*}\delta\Big[\frac{7}{36}\cos(\theta) + \frac{1}{36}\cos(3\theta) + \frac{1}{72}\cos(\theta)e^{-6\tau} - \frac{1}{72}\cos(3\theta)e^{-6\tau} - \frac{1}{6}\cos(\theta)\tau - \frac{43}{200}\cos(\theta)e^{-2\tau} \\ + \frac{1}{150}\,\cos(\theta)e^{-12\,\tau} + \frac{1}{90}\,e^{-12\,\tau}\cos(3\,\theta) - \frac{1}{40}\,\cos(3\,\theta)e^{-2\,\tau} - \frac{1}{10}\,\cos(\theta)\tau\,e^{-2\,\tau}\Big] \qquad \text{(A.3)}$$

and the fourth moment

$$
\begin{aligned}
\left\langle \frac{(x(t)-x_0)^4}{(D_a/D_r)^2} \right\rangle = \tau^2 \Bigg[& 1/3\, F_e^{*4} + 4\, F_e^{*2}(1-1/2\,\delta) - 4\,\delta\,(1-1/2\,\delta) \\
& - \frac{295147905179352817853}{442721857769029238784}\, F_e^{*2}\delta + 12\,(1-1/2\,\delta)^2 + 1/3\,\delta^2 \Bigg] \\
& + \tau \Bigg[6\, F_e^{*2}\delta \left(\frac{16971004547812787156293}{79689934398425262981120} + \frac{184467440737095508157}{55782954078897684086784}\, e^{-6\,\tau} \right. \\
& \quad + \frac{184467440737095508157}{18594318026299228028928}\, \cos(2\,\theta) e^{-6\,\tau} + \frac{230584300921369395}{9223372036854775808}\, e^{-2\,\tau} \\
& \quad \left. - \frac{230584300921369395}{9223372036854775808}\, \cos(2\,\theta) e^{-2\,\tau} + \frac{147573952589676420931}{5312662293228350865408}\, \cos(2\,\theta) \right) \\
& + 3\,\delta^2 \left(-1/9\, \cos(2\,\theta) + \frac{11}{135} - \frac{1}{189}\, e^{-6\,\tau} - \frac{1}{63}\, \cos(2\,\theta) e^{-6\,\tau} \right) \\
& + F_e^{*4} \left(\frac{3}{20}\, \cos(2\,\theta) e^{-2\,\tau} + 1/6\, \cos(2\,\theta) - \frac{3}{20}\, e^{-2\,\tau} - \frac{1}{252}\, e^{-6\,\tau} - \frac{1}{84}\, \cos(2\,\theta) e^{-6\,\tau} - \frac{47}{90} \right) \\
& + 1/6\, F_e^{*2}(1-1/2\,\delta) \left(-10 + 6\, \cos(2\,\theta) + 9\, e^{-2\,\tau} - 9\, \cos(2\,\theta) e^{-2\,\tau} + 3\, \cos(2\,\theta) e^{-6\,\tau} + e^{-6\,\tau} \right) \\
& + 2/3\,\delta\,(1-1/2\,\delta) \left(3\, \cos(2\,\theta) + 1 - 3\, \cos(2\,\theta) e^{-6\,\tau} - e^{-6\,\tau} \right) \Bigg] \\
& + F_e^{*4} \Bigg[\frac{1}{2400}\, \cos(2\,\theta) e^{-12\,\tau} + \frac{1}{9600}\, e^{-12\,\tau} + \frac{1}{672}\, \cos(4\,\theta) e^{-6\,\tau} - \frac{4}{441}\, \cos(2\,\theta) e^{-6\,\tau} \\
& \quad - \frac{121}{720}\, \cos(2\,\theta) - \frac{1}{480}\, \cos(4\,\theta) e^{-2\,\tau} + \frac{53}{300}\, \cos(2\,\theta) e^{-2\,\tau} + \frac{1}{960}\, \cos(4\,\theta) \\
& \quad + \frac{11}{14112}\, e^{-6\,\tau} + \frac{4901}{14400} + \frac{1411740617885935}{73786976294838206464}\, e^{-20\,\tau} - \frac{273}{800}\, e^{-2\,\tau} \\
& \quad + \frac{1}{23520}\, e^{-20\,\tau} \cos(2\,\theta) - \frac{1}{1920}\, \cos(4\,\theta) e^{-12\,\tau} + \frac{1}{13440}\, e^{-20\,\tau} \cos(4\,\theta) \Bigg] \\
& + 6\, F_e^{*2}\delta \Bigg[\frac{304002342334733405771}{2361183241434822606848}\, e^{-2\,\tau} + \frac{1475739525896763653647}{318759737593701051924480}\, \cos(2\,\theta) \\
& \quad + \frac{26235369349275805845}{18889465931478580854784}\, \cos(4\,\theta) e^{-12\,\tau} - \frac{5247073869855161169}{18889465931478580854784}\, e^{-12\,\tau} \\
& \quad + \frac{491913175298921373631}{14167099448608935641088 0}\, \cos(4\,\theta) + \frac{24595658764946071489}{4958484807013127474380 8}\, \cos(4\,\theta) e^{-6\,\tau} \\
& \quad + \frac{29809938423114633542725}{31238454284182703088599 04}\, \cos(2\,\theta) e^{-6\,\tau} - \frac{807229520665529965278287}{63751947518740210384896 00} \\
& \quad - \frac{271536072765004556323}{21250649172913403461632}\, \cos(2\,\theta) e^{-2\,\tau} - \frac{807045053224792883}{166020696663385964544}\, \cos(4\,\theta) e^{-2\,\tau} \\
& \quad - \frac{295147905179352818 5637}{23139595766061261547110400}\, e^{-20\,\tau} - \frac{295147905179352818 5637}{10412818094727567696199680}\, e^{-20\,\tau} \cos(2\,\theta) \\
& \quad - \frac{5247073869855161169}{4722366482869645213696}\, \cos(2\,\theta) e^{-12\,\tau} - \frac{295147905179352818 5637}{59501817684157529692569 60}\, e^{-20\,\tau} \cos(4\,\theta) \\
& \quad - \frac{673306158690398658161}{39048067855228378860748 8}\, e^{-6\,\tau} \Bigg] \\
& + 3\,\delta^2 \Bigg[\frac{1}{280}\, e^{-20\,\tau} \cos(4\,\theta) + \frac{1}{490}\, e^{-20\,\tau} \cos(2\,\theta) - \frac{1}{84}\, \cos(4\,\theta) e^{-6\,\tau} - \frac{19}{1800} - \frac{37}{1323}\, \cos(2\,\theta) e^{-6\,\tau} \\
& \quad + \frac{1}{120}\, \cos(4\,\theta) + \frac{7}{270}\, \cos(2\,\theta) + \frac{17}{1764}\, e^{-6\,\tau} + \frac{9}{9800}\, e^{-20\,\tau} \Bigg] . \qquad \text{(A.4)}
\end{aligned}
$$

[1] J. Toner, Y. Tu, and S. Ramaswamy, Annals of Physics, **318**, 170 (2005).
[2] E. Lauga and T. R. Powers, Rep. Prog. Phys., **72**, 096601 (2009).
[3] H. C. Berg and D. A. Brown, Nature, **239**, 500 (1972).
[4] H. C. Berg and L. Turner, Biophys. J., **58**, 919 (1990).
[5] W. R. DiLuzio, L. Turner, M. Mayer, P. Garstecki, D. B. Weibel, H. C. Berg, and G. M. Whitesides, Nature, **435**, 1271 (2005).
[6] E. Lauga, W. R. DiLuzio, G. M. Whitesides, and H. A. Stone, Biophys. J., **90**, 400 (2006).
[7] J. Hill, O. Kalkanci, J. L. McMurry, and H. Koser, Phys. Rev. Lett., **98**, 068101 (2007).
[8] V. B. Shenoy, D. T. Tambe, A. Prasad, and J. A. Theriot, PNAS, **104**, 8229 (2007).
[9] J. Tailleur and M. E. Cates, Europhys. Lett., **86**, 60002 (2009).
[10] K. C. Leptos, J. S. Guasto, J. P. Gollub, A. I. Pesci, and R. E. Goldstein, Phys. Rev. Lett., **103**, 198103 (2009).
[11] I. H. Riedel, K. Kruse, and J. Howard, Science, **309**, 300 (2005).
[12] D. M. Woolley, Reproduction, **126**, 259 (2003).
[13] B. M. Friedrich and F. Jülicher, New J. Phys., **10**, 123025 (2008).
[14] P. Dhar, T. M. Fischer, Y. Wang, T. E. Mallouk, W. F. Paxton, and A. Sen, Nano Lett., **6**, 66 (2006).
[15] A. Walther and A. H. E. Müller, Soft Matter, **4**, 663 (2008).
[16] A. Erbe, M. Zientara, L. Baraban, C. Kreidler, and P. Leiderer, J. Phys.: Condens. Matter, **20**, 404215 (2008).
[17] L. Baraban, C. Kreidler, D. Makarov, P. Leiderer, and A. Erbe, (2008), arXiv:0807.1619v1.
[18] R. Golestanian, Phys. Rev. Lett., **102**, 188305 (2009).
[19] M. N. Popescu, S. Dietrich, and G. Oshanin, J. Chem. Phys., **130**, 194702 (2009).
[20] R. Dreyfus, J. Baudry, M. L. Roper, M. Fermigier, H. A. Stone, and J. Bibette, Nature, **437**, 862 (2005).
[21] A. Ghosh and P. Fischer, Nano Lett., **9**, 2243 (2009).
[22] M. Belkin, A. Snezhko, I. S. Aranson, and W.-K. Kwok, Phys. Rev. E, **80**, 011310 (2009).
[23] S. Schmidt, J. van der Gucht, P. M. Biesheuvel, R. Weinkamer, E. Helfer, and A. Fery, Eur. Biophys. J., **37**, 1361 (2008).
[24] A. Kudrolli, G. Lumay, D. Volfson, and L. S. Tsimring, Phys. Rev. Lett., **100**, 058001 (2008).
[25] L. J. Daniels, Y. Park, T. C. Lubensky, and D. J. Durian, Phys. Rev. E, **79**, 041301 (2009).
[26] D. W. Howell, I. S. Aronson, and G. W. Crabtree, Phys. Rev. E, **63**, 050301(R) (2001).
[27] T. Obata, T. Shimizu, H. Osaki, H. Oshima, and H. Hara, J. Korean Phys. Soc., **46**, 713 (2005).
[28] C. Castellano, S. Fortunato, and V. Loreto, Rev. Mod. Phys., **81**, 591 (2009).
[29] J. Dunkel and I. M. Zaid, Phys. Rev. E, **80**, 021903 (2009).
[30] It is important to note that the motion of swimmers is force-free. Hence the force entering into the Langevin equation is an effective one which describes the propulsion mechanism on average.
[31] V. Lobaskin, D. Lobaskin, and I. M. Kulić, Eur. Phys. J. Special Topics, **157**, 149 (2008).
[32] S. van Teeffelen and H. Löwen, Phys. Rev. E, **78**, 020101(R) (2008).
[33] Alternatively, self-propelled particles have been modeled by damped Brownian dynamics with a Rayleigh friction term [67] or by prescribing a velocity field on the surface of the particle due to surface deformations [68].
[34] M. Doi and S. F. Edwards, *The Theory of Polymer Dynamics* (Oxford Science Publications, Oxford, 1986).
[35] H. Löwen, Phys. Rev. E, **50**, 1232 (1994).
[36] T. Kirchhoff, H. Löwen, and R. Klein, Phys. Rev. E, **53**, 5011 (1996).
[37] Y. Han, A. M. Alsayed, M. Nobili, J. Zhang, T. C. Lubensky, and A. G. Yodh, Science, **314**, 626 (2006).
[38] Y. Han, A. Alsayed, M. Nobili, and A. G. Yodh, Phys. Rev. E, **80**, 011403 (2009).
[39] G. Nägele, Phys. Rep., **272**, 215 (1996).
[40] A. Einstein, Ann. Phys. (Leipzig), **19**, 289 (1906).
[41] F. Perrin, J. Phys. Radium, **5**, 497 (1934).
[42] F. Perrin, J. Phys. Radium, **7**, 1 (1936).
[43] C. Ribrault, A. Triller, and K. Sekimoto, Phys. Rev. E, **75**, 021112 (2007).
[44] R. Grima and S. N. Yaliraki, J. Chem. Phys., **127**, 084511 (2007).
[45] J. K. G. Dhont, *An Introduction to Dynamics of Colloids* (Elsevier, Amsterdam, 1996).
[46] T. Munk, F. Höfling, E. Frey, and T. Franosch, Europhys. Lett., **85**, 30003 (2009).
[47] S. R. Aragón S. and R. Pecora, J. Chem. Phys., **82**, 5346 (1985).
[48] J. Elgeti and G. Gompper, Europhys. Lett., **85**, 38002 (2009).
[49] Y.-G. Tao, W. K. den Otter, J. T. Padding, J. K. G. Dhont, and W. J. Briels, J. Chem. Phys., **122**, 244903 (2005).
[50] B. ten Hagen, S. van Teeffelen, and H. Löwen, Condensed Matter Physics, **12**, 725 (2009).
[51] C. Lutz, M. Kollmann, and C. Bechinger, Phys. Rev. Lett., **93**, 026001 (2004).
[52] R. D. L. Hanes, M. C. Jenkins, and S. U. Egelhaaf, Rev. Sci. Instr., **80**, 083703 (2009).
[53] We note that, due to the independence of the initial configuration, Eq. (34) can also be derived directly from the correlation function $\langle \hat{u}(t) \cdot \hat{u}_0 \rangle = \exp(-2D_r t)$ [34].
[54] G. P. Alexander, C. M. Pooley, and J. M. Yeomans, J. Phys.: Condens. Matter, **21**, 204108 (2009).
[55] K. Drescher, K. C. Leptos, I. Tuval, T. Ishikawa, T. J. Pedley, and R. E. Goldstein, Phys. Rev. Lett., **102**, 168101 (2009).
[56] A. P. Berke, L. Turner, H. C. Berg, and E. Lauga, Phys. Rev. Lett., **101**, 038102 (2008).
[57] B. M. Friedrich and F. Jülicher, Phys. Rev. Lett., **103**, 068102 (2009).
[58] J. Strefler, W. Ebeling, E. Gudowska-Nowak, and L. Schimansky-Geier, Eur. Phys. J. B, **72**, 597 (2009).
[59] B. Lindner and E. M. Nicola, Phys. Rev. Lett., **101**, 190603 (2008).
[60] P. Galajda, J. Keymer, P. Chaikin, and R. Austin, J. Bacteriol., **189**, 8704 (2007).
[61] M. B. Wan, C. J. O. Reichhardt, Z. Nussinov, and C. Reichhardt, Phys. Rev. Lett., **101**, 018102 (2008).

[62] F. Höfling, T. Munk, E. Frey, and T. Franosch, J. Chem. Phys., **128**, 164517 (2008).
[63] F. Höfling, T. Munk, E. Frey, and T. Franosch, Phys. Rev. E, **77**, 060904(R) (2008).
[64] P. Romanczuk, I. D. Couzin, and L. Schimansky-Geier, Phys. Rev. Lett., **102**, 010602 (2009).
[65] H. H. Wensink and H. Löwen, Phys. Rev. E, **78**, 031409 (2008).
[66] F. Peruani, A. Deutsch, and M. Bär, Phys. Rev. E, **74**, 030904(R) (2006).
[67] U. Erdmann, W. Ebeling, and V. S. Anishchenko, Phys. Rev. E, **65**, 061106 (2002).
[68] M. T. Downton and H. Stark, J. Phys.: Condens. Matter, **21**, 204101 (2009).